https://doi.org/10.5194/egusphere-2026-571
Preprint. Discussion started: 12 February 2026

The Role of Rossby Wave Breaking in the Formation and Maintenance of Tropical-Extratropical Cloud Bands over the South Pacific

Romain Pilon[1], Andries Jan De Vries[1], and Daniela I.V. Domeisen[1, 2]

[1]Institute of Earth Surface Dynamics, University of Lausanne, Lausanne, Switzerland
[2]Institute for Atmospheric and Climate Science, ETH Zürich, Zürich, Switzerland

Correspondence: Romain Pilon (romain.pilon@unil.ch)

Abstract. Tropical-extratropical cloud bands are elongated cloud structures bridging tropical and midlatitude regions that act as a primary source of regional precipitation. While the role of Rossby wave breaking in the formation of cloud bands is established, the extent to which this dynamic forcing governs cloud band characteristics, their entire lifecycle, their spatial distribution and seasonality has not yet been systematically quantified. In this study, we apply an object-based approach to reanalysis data to investigate how stratospheric potential vorticity (PV) structures, as indicators of Rossby wave breaking, influence cloud band formation and persistence over the South Pacific region. Our climatological analysis confirms a robust statistical link in which cyclonic PV structures steer tropical moisture poleward and eastward, shaping the diagonal orientation of the cloud bands. We also find that cloud band duration is modulated by the properties of PV structures: long-lived cloud bands are distinguished by a systematically higher frequency of upstream PV structures and are sustained by persistent PV structures throughout their lifecycle, which favour a more zonal orientation of the cloud systems. Categorizing by cloud band duration reveals distinct seasonal regimes: while short-lived events occur year-round, persistent cloud bands are strictly confined to the austral warm season. Furthermore, long-lived cloud bands are associated with PV structures that reside significantly farther equatorward prior to genesis compared to those of short-lived events. These findings highlight that equatorward-breaking Rossby waves create a tropospheric environment favouring not only the formation but also the maintenance of these cloud bands. Consequently, accurately representing Rossby wave dynamics in weather and climate models is critical for simulating cloud band characteristics and their influence on climate variability.

1 Introduction

The South Pacific Convergence Zone (SPCZ) is the most prominent rain band in the Southern Hemisphere and a dominant feature of the global climate system. Together with the South Atlantic Convergence Zone (SACZ) and the South Indian Convergence Zone (SICZ), it forms one of the three primary diagonal convective bands in the Southern Hemisphere (Kodama, 1992; van der Wiel et al., 2015). Extending southeastward from the tropical western Pacific into the central subtropical Pacific, the SPCZ comprises a zonally orientated tropical component and a diagonally orientated subtropical segment (Vincent, 1994; Brown et al., 2020). Climatologically, the SPCZ represents the aggregation of recurring, synoptic-scale precipitating cloud

https://doi.org/10.5194/egusphere-2026-571
Preprint. Discussion started: 12 February 2026

bands. These cloud bands play a critical dual role in the regional hydroclimate. On one hand, they act as the primary freshwater source for many Pacific Island nations, supporting agriculture and local economies (Griffiths et al., 2003; Kumar et al., 2006). On the other hand, they are frequently associated with hydro-meteorological extremes; their variability – particularly when events become stationary or intense – is a primary driver of both droughts and devastating flooding (Lorrey et al., 2012; Brown et al., 2020; Sagero et al., 2024). Given the impact of these systems on the atmospheric and hydroclimatic conditions in the South Pacific, it is crucial to understand the dynamic factors governing not only their formation, lifetime, spatial and seasonal distribution but also their evolution and intensity.

The existence and position of the SPCZ are largely controlled by the distribution of sea surface temperatures and the zonal asymmetry of the atmospheric background flow (Takahashi and Battisti, 2007; Widlansky et al., 2011). This background state varies on intraseasonal to interannual timescales due to the influence of the MJO and ENSO (Matthews et al., 1996; Brown et al., 2020). Furthermore, the characteristic diagonal orientation of the SPCZ is shaped by the propagation of Rossby waves from the extratropics; idealized dynamical frameworks have demonstrated that these waves are refracted toward the equatorial westerly duct, a process that organizes convection into the distinct northwest–southeast tilt observed in the climatology (Matthews, 2012; van der Wiel et al., 2015, 2016). Consequently, the variability of the SPCZ, particularly in its southern extent, is strongly modulated by the breaking of these midlatitude Rossby waves and the resulting tropical–extratropical interactions (Kiladis, 1998; Allen et al., 2009; Niznik et al., 2015).

Rossby wave breaking (RWB) is dynamically defined by the rapid, irreversible overturning of potential vorticity (PV) contours on isentropic surfaces (McIntyre and Palmer, 1983). In this study, we identify these breaking events by detecting their characteristic morphology: elongated intrusions of stratospheric high-PV air – known as PV streamers (Appenzeller and Davies, 1992) – that penetrate the tropical upper troposphere and may detach to form isolated PV cut-offs (Wernli and Sprenger, 2007). These PV intrusions destabilize the lower atmosphere and induce ascent, thereby facilitating deep convection (Funatsu and Waugh, 2008; Waugh and Funatsu, 2003; Allen et al., 2009). Simultaneously, the cyclonic circulation associated with PV intrusions transports tropical moisture poleward and eastward along their downstream flank, often contributing to the formation of atmospheric rivers and to the development of tropical–extratropical cloud bands (Knippertz and Martin, 2005; de Vries et al., 2018), particularly in regions of westerly flow (Knippertz, 2007; Stan et al., 2017).

Cloud bands resulting from such interactions – also referred to in the literature as tropical plumes – have been identified in various regions, including South America (Rosa et al., 2020; Zilli and Hart, 2021; Zilli et al., 2023), Southern Africa (Hart et al., 2013), northwestern Africa (Knippertz and Martin, 2005), Australia (Telcik and Pattiaratchi, 2014; Black et al., 2021), and the Middle East (Tubi and Dayan, 2014). Among these regions, the South Pacific stands out: global objective climatologies identify it as hosting the highest frequency and most spatially extensive tropical plumes on Earth (Fröhlich et al., 2013). Despite this prominence, the factors governing the lifecycle and duration of South Pacific cloud bands remain less characterized than those of their South Atlantic counterparts. For the SACZ, recent object-based studies have explicitly distinguished between transient and persistent events, demonstrating that long-lived cloud bands are actively sustained by amplified, recurrent Rossby wave trains (Zilli and Hart, 2021).

https://doi.org/10.5194/egusphere-2026-571
Preprint. Discussion started: 12 February 2026

In the South Pacific, while the fundamental role of Rossby waves in organizing the diagonal SPCZ is established through case studies and idealized experiments (Kiladis, 1998; Knippertz, 2007; van der Wiel et al., 2015, 2016), and its broad variability is well-documented (Brown et al., 2020), the specific dependency of cloud band lifetime on the properties of upstream wave forcing remains unquantified. Most existing climatological assessments rely on instantaneous co-occurrence statistics or fixed-grid analyses (e.g., Kiladis, 1998; Fröhlich et al., 2013; Brown et al., 2020), leaving the coupled lifecycle evolution of these systems unresolved. Consequently, it remains an open question whether the lifetime of these cloud bands is primarily dictated by the large-scale background flow, or if it is actively modulated by the properties of the triggering PV intrusions, such as their vertical depth and meridional extent.

To address this gap, we quantify the climatological statistics of the coupling between PV intrusions and cloud bands in the South Pacific and characterize their spatial and temporal variability. Furthermore, we hypothesize that the duration of these cloud bands is influenced by the properties of their dynamic drivers; for instance, that sustained and vertically extensive (deep) PV structures provide a more favourable environment for moisture transport and enhanced convection, thereby supporting longer-lived cloud bands. To test this hypothesis, we employ a cloud band tracking algorithm to follow events through their full lifecycle. This object-based approach allows for a robust climatological analysis of the connection between cloud band events and their dynamic drivers, providing insights into the drivers of cloudiness over the SPCZ.

2 Data and Methods

We use the ERA5 global reanalysis dataset (Hersbach et al., 2020) from the European Centre for Medium-Range Weather Forecasts (ECMWF) for the period 1959–2021, on a 0.5-degree regular grid, to identify cloud bands and PV structures.

2.1 Identification and Tracking of Tropical-Extratropical Cloud Bands and PV Structures

2.1.1 Identification of Cloud Bands

Tropical-extratropical cloud bands in the South Pacific are identified using the detection algorithm of Pilon and Domeisen (2024), which applies an image segmentation approach to outgoing longwave radiation (OLR) fields using a threshold of $210\,\mathrm{W\,m^{-2}}$. Contiguous regions with OLR values below this threshold are defined as distinct cloud objects. To isolate tropical-extratropical interactions, the algorithm filters for objects satisfying specific geometric criteria: cloud bands must cross 23.5° north or south, must exhibit a diagonal orientation and extend from tropical latitudes (equatorward of 20°S) into the mid-latitudes (poleward of 27°S).

The detection is restricted to a domain encompassing the SPCZ (130°E–70°W, 5°N–50°S). This spatial constraint is critical to minimize the identification of artefacts; otherwise, the algorithm risks erroneously merging the SPCZ with the intertropical convergence zone or with mid-latitude cold clouds, resulting in the false detection of extensive cloud bands (Pilon and Domeisen, 2024). For this study, the detection is performed on daily mean OLR fields derived from the 3-hourly ERA5 data.

https://doi.org/10.5194/egusphere-2026-571
Preprint. Discussion started: 12 February 2026

This temporal averaging acts as a smoothing procedure that improves the connectivity between low-OLR regions, thereby preventing the over-segmentation of cloud systems.

2.1.2 Spatio-temporal Tracking of Cloud Bands

To facilitate the climatological analysis of transient cloud bands and their precursors, an event-based tracking algorithm is developed. This approach extends the daily detection and frame-to-frame inheritance tracking of Pilon and Domeisen (2024). This framework allows us to perform composite analyses centred on specific lifecycle stages (e.g., genesis) and quantify event characteristics, such as duration, for correlation with upstream PV structures.

The genesis of a new cloud band event is defined when a cloud band is detected at a time t without a spatially overlapping structure at the previous time step $(t-1)$. Temporal continuity is maintained when a cloud band corresponds to a single antecedent structure that, in turn, evolves into only that single subsequent structure. When a single cloud band at a time t is found to have spatial overlap with multiple distinct antecedent structures at a day $t-1$ (as it can occur when a tropical moisture plume and a mid-latitude front merge) the cloud band inherits the event identification of the oldest (longest-lived) antecedent event. Conversely, when a single antecedent structure evolves into multiple distinct cloud bands – for instance, when cloud systems associated with a front detach from the tropical part of the SPCZ – this defines the end of the event. This criterion is critical for isolating coherent structures, as each resulting structure subsequently initiates a new, independent event, thereby avoiding the ambiguity of defining a single entity through complex evolutions.

This event-based framework yields a dataset of discrete cloud band events, each with a defined genesis, end, and duration.

2.1.3 Categorization of Cloud Band Duration

Based on the tracking output, the duration T of a cloud band event is defined as the number of consecutive days between its genesis and end. To characterize the typical lifecycles of these systems, we compute the empirical survival function, which estimates the probability that a cloud band's duration T exceeds a specific number of t days. For a total population of N events, this is calculated as:

$$P(T > t) = \frac{1}{N} \sum_{i=1}^{N} \mathbb{1}(d_i > t)$$

where d_i is the duration of the i-th event and $\mathbb{1}(\cdot)$ is the indicator function (taking the value of 1 if the condition is met and 0 otherwise). Table 1 presents these survival probabilities for the 1959–2021 period. The distribution is highly skewed towards short-duration events; approximately 42% of cloud bands last for only one day, and only 10% persist for longer than 5 days.

To differentiate the dynamic environments driving these lifecycles, we stratify cloud bands into three categories based on these survival probabilities: transient (1–2 days; representing ∼65% of the population), "transitional" (3 days), and persistent ($\geq$ 4 days; representing the top ∼15% of lifetime). This 4-day threshold for persistence is consistent with the methodology used for South American cloud bands by Zilli and Hart (2021). As the 3- day events represent a transition zone with mixed

https://doi.org/10.5194/egusphere-2026-571
Preprint. Discussion started: 12 February 2026

dynamic characteristics, the following comparative analysis focuses on the contrast between the distinct transient and persistent regimes.

Table 1. Empirical survival probabilities for cloud band lifetimes for the period 1959-2021. The values indicate the percentage of events with a duration (T) strictly exceeding t days.

Duration t (days)	1	2	3	4	5	7	10
$P(T > t)$ (%)	57.9	35.4	22.8	14.8	10.1	5.1	1.9

2.2 Identification of Stratospheric Potential Vorticity Structures

We use PV structures as indicators of Rossby wave breaking using the algorithm of de Vries et al. (2018, 2024), adapted from Wernli and Sprenger (2007). PV is computed from 6-hourly data on ERA5 model levels and then linearly interpolated onto isentropic levels between 295 and 370 K at 5 K intervals. The method uses 2 potential vorticity unit (PVU; where $1\,\mathrm{PVU} = 10^{-6}\,\mathrm{K\,kg^{-1}\,m^2\,s^{-1}}$) contours, representing the dynamical tropopause, which separates stratospheric and tropospheric air masses, to identify PV streamers and cut-off lows, hereafter referred to as PV structures. Here, we only use stratospheric PV structures with $|\mathrm{PV}| > 2\,\mathrm{PVU}$. To ensure temporal consistency with the cloud band dataset, we aggregate these 6-hourly PV features onto a daily timescale. Furthermore, we specifically define "deep PV structures" as grid points having PV structures for at least three consecutive time steps (i.e., 18 hours) and spanning at least two isentropic levels. These deep PV structures are illustrated in Figure 1 as the number of isentropic levels with such detected features.

2.3 Connection Between PV Structures and Cloud Bands

2.3.1 Collocation Methodology

To quantify how many cloud bands are associated with PV structures and to assess their spatial relationship, we use a collocation method based on the geometrical bounding boxes and centroids (which are here the weighted centre of mass) of both features (details are provided in the supplementary information). Both cloud bands and PV structures are analysed on a daily timescale. To prevent over-attribution of cloud bands to PV structures, given their relatively high frequency and large spatial extents, we select only the deep PV structures defined in Sect. 2.2 (i.e., those that are both sufficiently deep and persistent). A cloud band is considered connected to a deep PV structure if their bounding boxes overlap and the centroid of the PV structure lies south-west of the cloud band's diagonal transect (Figure A1). This geometric constraint is applied to capture the specific dynamical configuration of tropical-extratropical interactions, in which the forcing upper-level trough is positioned at the upstream flank of the cloud band.

https://doi.org/10.5194/egusphere-2026-571
Preprint. Discussion started: 12 February 2026

2.3.2 Composite Analysis

To characterize atmospheric conditions throughout the cloud band lifecycle, we construct spatial composites within a 6000×6000 km domain centred on the cloud band's centroid (see Sect. 3.3). This analysis focuses on PV structure depth (defined as the mean number of isentropic levels with PV structures), OLR, integrated water vapour transport (IVT), and anomalies of geopotential height at 500 hPa (Z500). The anomalies are computed relative to a long-term (1959–2021) climatology based on a 21-day running mean of daily averages to remove the seasonal cycle, following the methodology of Hart and Grumm (2001) and de Vries et al. (2016).

For the quantitative analysis of upstream PV structures (and the creation of lagged time series), we define a dynamic "upstream sector". This sector is defined as the triangular area to the southwest of the cloud band, bounded by its geometric bounding box and the feature's major axis (Figure A1). This adaptive-area approach is designed to select PV structures located near the cloud band's genesis region and poleward flank, filtering out far-upstream mid-latitude signals. For lagged analyses centred on the time of event genesis ($t = 0$), this upstream sector is fixed relative to the genesis location for all negative lags ($t \leq 0$) and follows the tracked cloud band centroid for all positive lags ($t > 0$).

2.3.3 Significance Testing

To assess the statistical significance of cloud band – PV connections, we perform a Monte Carlo (MC)-based significance test. We generate 5000 randomized datasets by shuffling the positions of deep PV structures in time, using random dates throughout the year without maintaining seasonality (e.g., a cloud band from October could be associated with a PV structure from May). For each MC simulation and for each grid point, we compute the fraction of cloud bands that are connected to randomized deep PV structures. We then calculate p-values as the fraction of MC simulations where the simulated connection is greater than or equal to the observed connection. A grid point is considered statistically significant if its p-value is below 0.05, indicating that the observed connection between a deep PV structure and a cloud band is unlikely to have occurred by chance.

3 Results

3.1 Case studies

We first present two case studies over the South Pacific, shown in Figure 1, to demonstrate the connection between cloud bands and PV intrusion. In both cases, the cloud bands exhibit the typical northwest–southeast tilt characteristic of tropical-extratropical interactions in this region. The first case study (Figure 1a-d) illustrates a cloud band event over the South Pacific in January 2017, coinciding with flooding in Tahiti that had notable societal impacts. According to the EM-DAT international disaster database (Delforge et al., 2024), this event affected 5000 people and caused 2.559 million USD in damages. On 20 January, a PV cut-off is present around 30°S, 150°W, and is joined the following day by PV streamers intruding into the central South Pacific, coincident with the cloud band extending poleward. These PV streamers subsequently transform into a PV cut-

https://doi.org/10.5194/egusphere-2026-571
Preprint. Discussion started: 12 February 2026

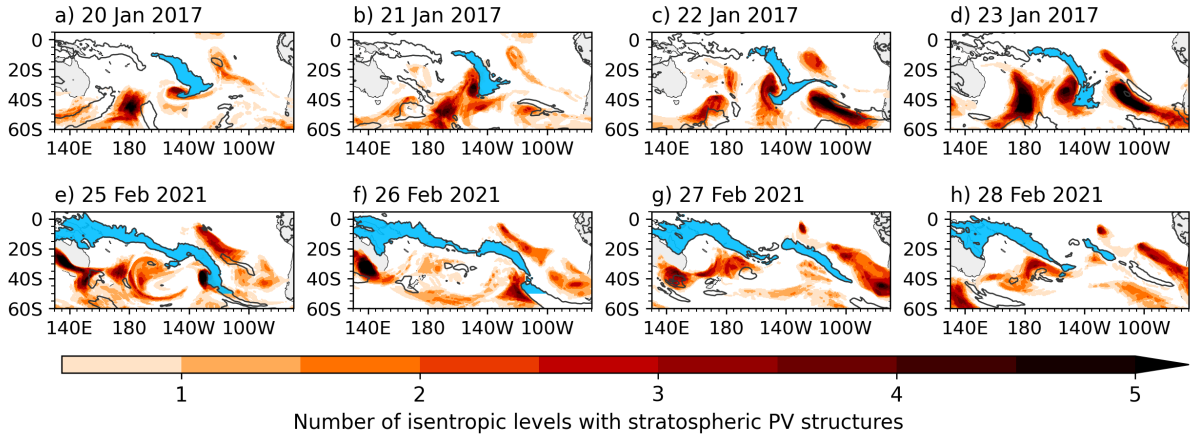

Figure 1. Daily snapshots of identified tropical-extratropical cloud bands (blue shading), daily mean of OLR at 210 W m^{-2} (black contour), and daily mean number of isentropic levels with stratospheric PV streamers and cut-offs (red shading) over the South Pacific for two distinct events: a-d) 20-23 January 2017, e-h) 25-28 February 2021.

off (around 35°S–150°W), associated with the further poleward elongation of the cloud band (Figure 1c-d). This evolution is consistent with the dynamics of tropical plumes induced by upper-level troughs described by Knippertz (2007).

A second example illustrates a different interaction between PV structures and cloud bands. The case study from February 2021 (Figure 1e-h) features a long cloud band exhibiting two sections: one zonally orientated in the tropics and the other diagonally orientated in the subtropics (Figure 1e-f). On 27 February, the cloud band split into two segments, influenced by two co-occurring PV structures, separated by approximately 60° of longitude (located at approximately (30°S, 180° and 35°S, 120°W). This splitting, driven by multiple PV intrusions and the resulting spatial separation between cloud structures, aligns with the interaction dynamics described by Kiladis and Weickmann (1992).

In both cases, PV structures are located to the west of tropical-extratropical cloud bands. This westward offset of PV structures relative to cloud bands is typical of the interactions observed in these events, where PV intrusions precede the development of tropical-extratropical cloud bands (Knippertz, 2007) and contribute to their diagonal orientation.

3.2 Climatologies

As a next step, to generalize beyond the case studies, we present the climatology of cloud bands and deep PV structures over the South Pacific from 1959 to 2021. Figure 2a presents the independent climatology of CBs and PV structures. The spatial distribution of cloud bands mirrors the SPCZ, being primarily concentrated in the central Pacific with a characteristic northwest–southeast orientation. This pattern resembles the climatology of tropical plumes described by Fröhlich et al. (2013). To the south, the frequency of PV structures exhibits a distinct meridional gradient, with occurrences increasing towards the extratropics. This aligns with the expected behaviour of Rossby wave breaking (RWB), occurs predominantly in the extratropics and reduces towards the tropics. This figure also illustrates PV structures extending further into the tropics in the eastern

https://doi.org/10.5194/egusphere-2026-571
Preprint. Discussion started: 12 February 2026

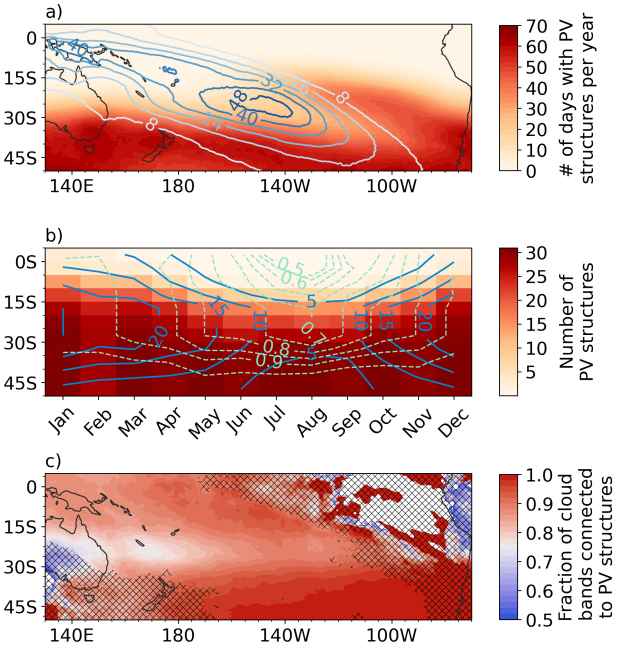

Figure 2. Climatologies of cloud bands and deep PV structures averaged between 1959 and 2021 across the South Pacific. (a) Annual average frequency of PV structures (shading) and cloud bands (contours) in days per year. The contours represent the average number of days with cloud bands per year during the same period. (b) Seasonal cycle as a function of latitude, where PV structures (shading) and cloud bands (solid contours) are integrated zonally across the domain and expressed as the average number of occurrences per month. The dashed contours show the fraction of cloud bands connected to deep PV structures (interval: 0.1). (c) Annual average fraction of cloud bands connected to deep PV structures; when 0% of cloud bands are linked to PV structures, values are masked out (white shading). Hatching indicates areas where the 5% significance level is not met, according to a Monte Carlo test.

Pacific, where westerly ducts are located. Westerly ducts facilitate interactions between extratropical westerlies and tropical flows, allowing Rossby waves to penetrate deeper into tropical latitudes (Webster and Holton, 1982; Waugh and Polvani, 2000; Knippertz, 2007; Fröhlich and Knippertz, 2008). Throughout the seasonal cycle, the occurrence of cloud bands aligns with the latitudinal migration of PV structures (Figure 2b), peaking when high PV structure frequencies extend equatorward during austral summer and autumn, consistent with the findings of Portmann et al. (2021). This alignment suggests that PV structures reaching farthest equatorward during the austral summer may facilitate interactions with tropical-extratropical cloud bands.

To quantify the broader linkage between PV structures and cloud bands, we analyse their spatial collocation, as defined in section 2.3. The spatial relationship between these features is shown in Figure 2c, which displays the average fraction of cloud bands connected to deep PV structures. The strongest connection and significant fractions are primarily observed in the central and eastern mid-latitudes of the basin, as well as in the western and central tropical Pacific. High fractions can also be found in the eastern tropical Pacific, but are not statistically significant due to the rare occurrence of cloud bands in this part of the

https://doi.org/10.5194/egusphere-2026-571
Preprint. Discussion started: 12 February 2026

ocean basin. The statistical significance test confirms that the region of robust connections aligns with the SPCZ and extends into the midlatitudes, highlighting the prevalence of tropical-extratropical interactions in the South Pacific.

3.3 Atmospheric Processes Contributing To Cloud Band Formation

While the fundamental mechanisms of tropical-extratropical interactions are established (e.g., Kiladis, 1998; Funatsu and Waugh, 2008), we first characterize the synoptic evolution specifically within our object-based framework to first validate that our tracking algorithm successfully captures the coherent physical coupling between Rossby wave breaking and convection described in the literature, and second, it defines the dynamical baseline required to understand the cloud band lifecycles discussed in the next section.

Figure 3 illustrates time-lagged composites of the synoptic environment centred on the cloud band onset (day 0). The composites (panels a–c) display the spatial distribution of PV structure depth, Z500 anomalies, OLR, and IVT for all cloud bands of the period. At day -2, an amplifying upper-level trough appears to the west of the future cloud band centroid, indicated by negative Z500 anomalies (dashed contours) and increased PV structure frequency. At this precursor stage, moisture transport (IVT) is dominated by the background easterly trade wind regime, and OLR values remain relatively high at the composite centre. By day 0, the interaction matures. The PV structure deepens and shifts to the south-west of the region of deep convection (low OLR). The PV dipole (high and low PV depths) is tilted northwest–southeast, matching the cloud band orientation. This configuration is consistent with anticyclonic RWB, typically associated with equatorward-moving upper-level troughs on the equatorward flank of the eddy-driven jet (Thorncroft et al., 1993). Near the equatorward edge of the PV structures, moisture is steered poleward along the eastern flank of the intrusion. By day +2, the dynamic forcing wanes: the PV structure becomes thinner, and the upstream trough fills (weakening Z500 anomalies), accompanied by a decrease in poleward moisture transport and the dissipation of the cloud band.

To examine the vertical structure of these interactions, we create vertical–meridional cross-sections of PV anomalies and vertical velocity (ω) centred on the centroid of cloud bands (Figure 3d–f). The composites reveal a strengthening dipole in the upper troposphere and lower stratosphere (300–100 hPa). A cyclonic PV anomaly (negative values, red shading) extends into the upper troposphere poleward of the cloud band centre, while an anticyclonic anomaly (positive values, blue shading) is positioned equatorward. From day -2 to day 0, this dipole intensifies. At onset (day 0), strong ascent (negative ω) is centred on the cloud band, located downstream of the cyclonic PV anomaly and along the poleward edge of the anticyclonic anomaly. This configuration is consistent with quasi-geostrophic forcing, where upper-level cyclonic PV anomalies destabilize the lower troposphere and induce upward motion ahead of the intrusion (Kiladis, 1998; Funatsu and Waugh, 2008). This structure highlights the influence of convective heating on the vertical PV distribution (Murthy and Boos, 2019): diabatic heating leads to the local destruction of PV above the heating maximum, creating or enhancing the anticyclonic anomaly (Oertel et al., 2020). Validating this feedback loop bridges the gap between the formation and evolution of cloud bands. It suggests that the duration of cloud bands is not solely a result of the initial trigger but rather is dynamically regulated by the persistence of this coupling.

https://doi.org/10.5194/egusphere-2026-571
Preprint. Discussion started: 12 February 2026

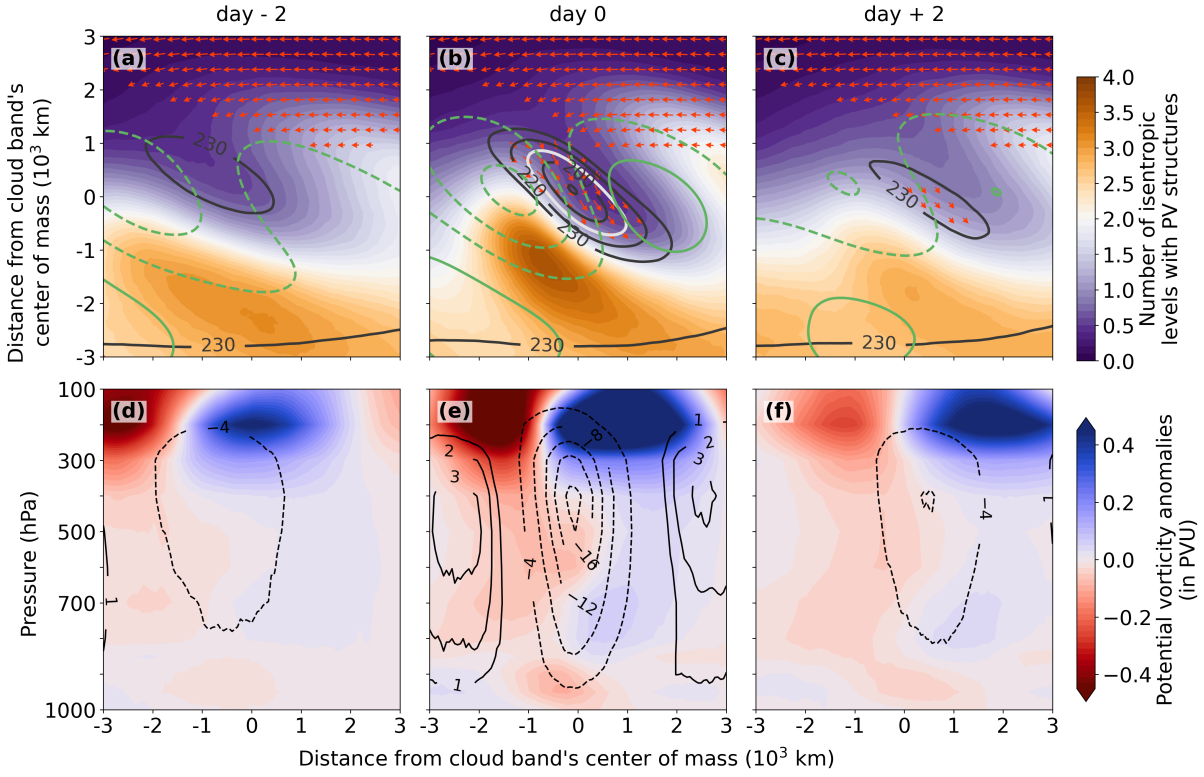

Figure 3. Time-lagged composites centred on the cloud band centroid for the period 1959–2021. The rows correspond to: (a)–(c) short-lived cloud bands; (d)–(f) persistent cloud bands; (g)–(i) all cloud bands; and (j)–(l) all cloud bands (vertical-meridional cross-section). Panels (a)–(i) show the daily mean of the vertical sum of isentropic levels with stratospheric PV structures (shading), OLR (solid black contours, in $\mathrm{W\,m^{-2}}$), normalized 500 hPa geopotential height anomalies (green contours; dashed for negative and solid for positive values; increment of 0.2 standard deviations, zero line omitted), and IVT (red arrows). IVT vectors are derived from their zonal and meridional components and are only displayed for magnitude values exceeding $150\,\mathrm{kg\,m^{-1}\,s^{-1}}$. Panels (j)-(l) show vertical–meridional cross-sections through the cloud band centroid, displaying vertical velocity ω (solid contours for positive values corresponding to descent, dashed contours for negative values corresponding to ascent, in $10^{-2}\,\mathrm{Pa\,s^{-1}}$) and PV anomalies (shading, in PVU). The white contour represents the $210\,\mathrm{W\,m^{-2}}$ cloud band detection threshold. Positive distances from cloud bands refer to positions north of the cloud band's centroid.

https://doi.org/10.5194/egusphere-2026-571
Preprint. Discussion started: 12 February 2026

3.4 Synoptic Controls on Cloud Band Duration

To characterize the factors influencing cloud band duration, we compare the synoptic evolution of short-lived ($\leq$ 2 days) and persistent ($\geq$ 4 days) events (Figure 4). While the vertical structure remains consistent across categories (not shown), the horizontal synoptic evolution reveals distinct differences in the upstream forcing. Differences are evident as early as the precursor stage (day -2). Persistent events are associated with existing cloudiness and an upstream trough (Figure 4d), whereas short-lived events show no precursor cloud signals and a weaker synoptic signature (Figure 4a). At onset (day 0), the contrast amplifies: persistent events are supported by a broad, intense upstream trough, indicated by large negative Z500 anomalies and coherent anomalies in PV structure frequencies. In contrast, short-lived events are flanked by a stronger downstream ridge (positive Z500 anomalies), which appears to confine the cloud bands spatially. By day +2, the dynamic forcing decays for short-duration cloud bands, evident from the dissipation of the anomalous PV structure frequencies (Figure 4c). The maintenance of a positive Z500 anomaly to the northeast of cloud bands suggests that the eastward propagation of the system is hindered by downstream ridging. Conversely, persistent events display deeper and more consistent anomalous PV structure frequencies than short-lived events (Figure 4f). Here, the circulation remains cyclonic, characterized by negative Z500 anomalies flanking the cloud band centre, providing continuous dynamical support to the system.

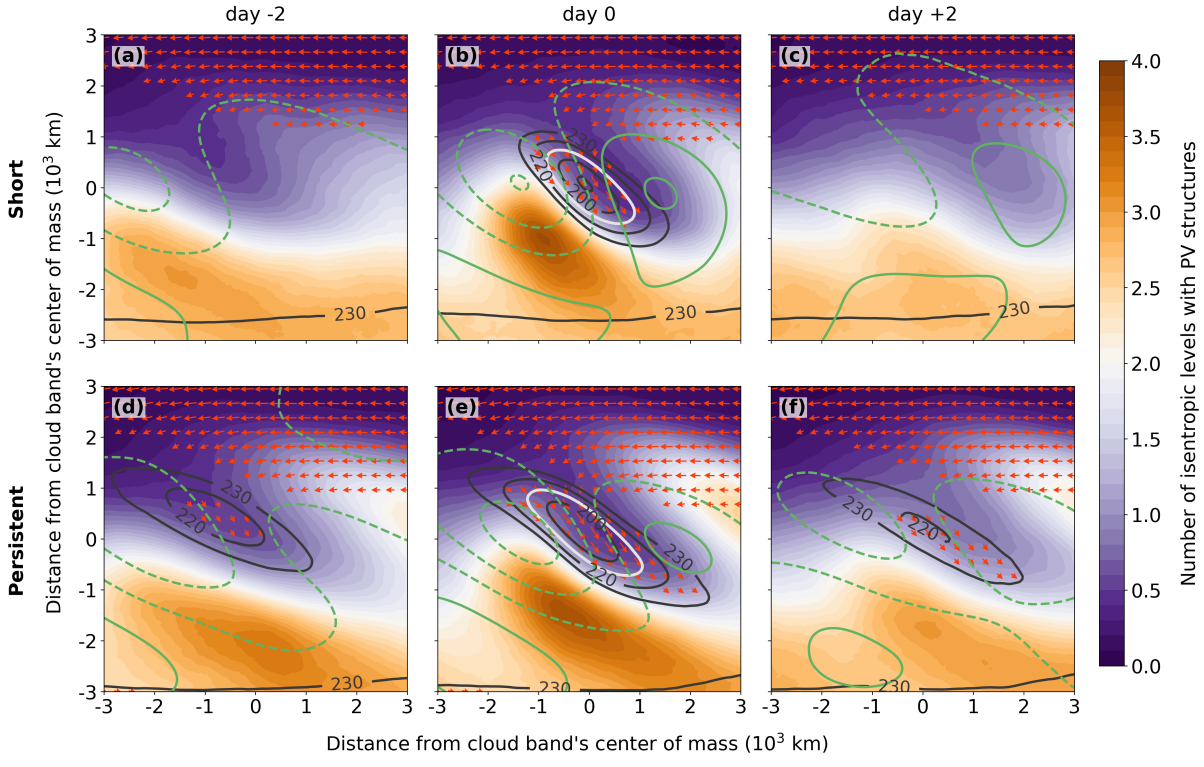

Figure 4. Same as Figure 3a–c but stratified by cloud band duration. (a)–(c): short-lived cloud bands (duration 1–2 days), and (d)–(f): persistent cloud bands (duration $\geq$ 4 days).

https://doi.org/10.5194/egusphere-2026-571
Preprint. Discussion started: 12 February 2026

3.5 Seasonality of Cloud Band Lifetime

To determine whether the lifetime of cloud bands has seasonal preferences, we analyse the seasonal cycle of short-lived versus persistent events (Figure 5) as a function of latitude. A clear distinction in seasonality with respect to lifetime becomes evident. Short-lived events (Figure 5a) display a broad seasonal distribution: While they exhibit a maximum in austral summer in the tropics, they occur throughout the year. This suggests that transient cloud bands can be triggered by Rossby wave breaking events throughout all seasons, having relevance to both summer tropical convection and winter transient frontal systems.

In contrast, persistent (long-lived) cloud bands (Figure 5b) are confined to the austral warm season, with a distinct frequency peak in the tropics during January and February and a notably lower frequency in the mid-latitudes. Frequencies subsequently drop to negligible values at all latitudes during austral winter (July–September). This implies that the maintenance of long-lived, quasi-stationary systems requires a specific concurrence of conditions: the sustained dynamic forcing of an upstream PV intrusion coupled with the favourable thermodynamic environment provided by the seasonal southward excursion of the ITCZ and tropical moisture (van der Wiel et al., 2016; Brown et al., 2020).

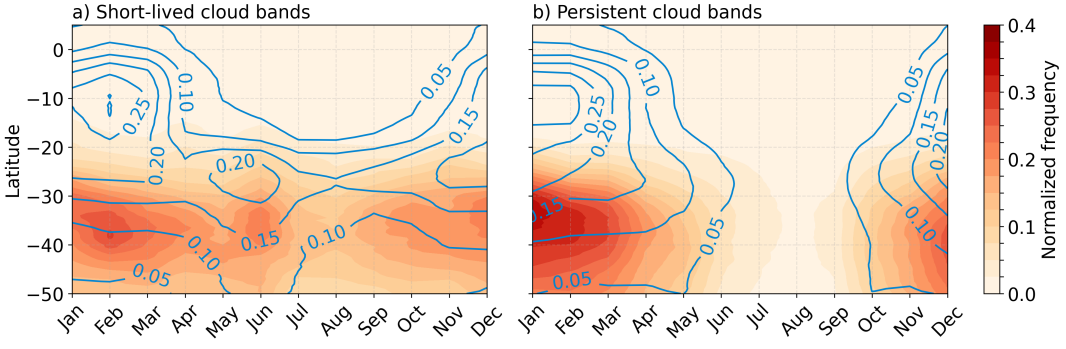

Figure 5. Seasonal cycle of zonal mean frequency for (a) short-lived and (b) persistent cloud bands (contours) and their connected PV structures (shading). Frequencies are normalized by the maximum value within each respective duration category (short-lived and persistent, respectively) to facilitate phase comparison.

3.6 Dynamic Drivers with Respect to Cloud Band Lifetime

To further identify the specific dynamic factors influencing cloud band lifecycles, we examine the characteristics of upstream PV structures. We focus on the contrast between the distinct transient and persistent cloud band categories (as defined in Sect. 2.1.3) to identify potential differences in the specific PV structures with respect to cloud band lifetime. The transitional category (duration of 3 days) is included in the figures as a reference to illustrate the intermediate behaviour between these two categories.

https://doi.org/10.5194/egusphere-2026-571
Preprint. Discussion started: 12 February 2026

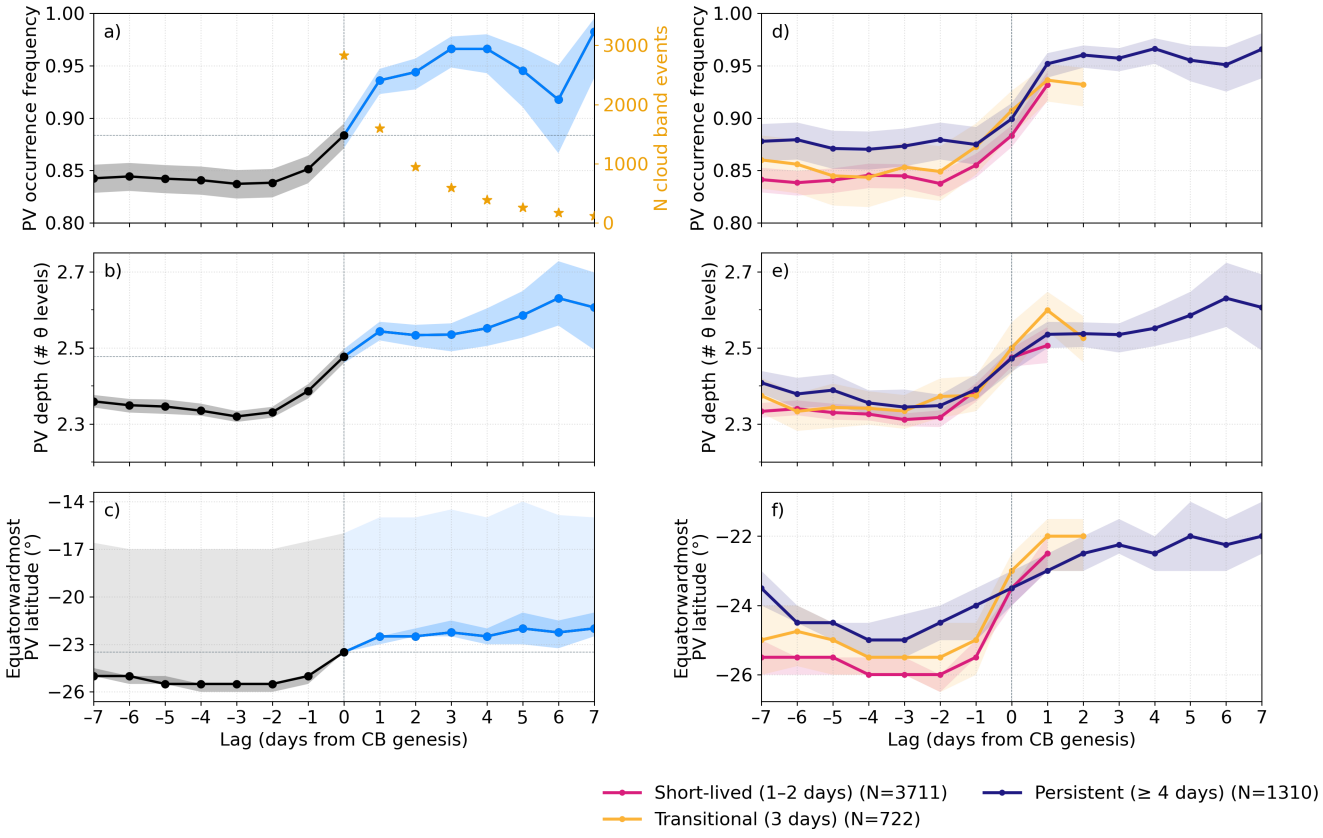

Figure 6. Time-lagged composites of PV characteristics relative to cloud band genesis (lag 0). All characteristics are computed within a dynamic upstream sector located south-west of the cloud band (see Sect. 2.3 for definition). The left column (a-c) shows composites for all events. The right column (d-f) stratifies these metrics by total cloud band duration, with the different line colours corresponding to the duration categories defined in the legend. The panels show: (a, d) the mean PV occurrence frequency (the proportion of cloud bands with an upstream PV structure); (b, e) the median vertical depth of the PV structure in isentropic (θ) levels; and (c, f) the median of the most equatorward latitude reached by the PV structures. In panels (a-c), the change from black to blue lines indicates a shift in the reference frame for the upstream sector: lags ≤ 0 (black) use a sector fixed relative to the genesis location, while lags > 0 (blue) follow the tracked cloud band centroid. The shading in these panels indicates the confidence interval: for (a, d), it is the 95% Wilson score confidence interval; for (b-f), the shading is the 95% bootstrap confidence interval for the median. Panel (c), in addition, includes light shading extending to the 90th percentile, quantifying the 10% most equatorward-penetrating PV intrusions. The right-hand axis and markers (yellow stars) in panel (a) show the number (total summed over all years) of individual cloud band events included at each lag.

https://doi.org/10.5194/egusphere-2026-571
Preprint. Discussion started: 12 February 2026

3.6.1 PV Structure Characteristics Upstream of Cloud Bands

To identify whether cloud band formation is driven by specific PV structures, Figure 6a presents a lead-lag plot of the composite frequency of PV structures within the upstream sector relative to cloud band genesis (corresponding to lag 0). The climatological baseline is high: even one week before genesis (lag -7), approximately 84% of future cloud band genesis locations already have a PV structure in their upstream sector. This high baseline is expected given the large spatial extent of the defined upstream sector, which naturally captures the high background frequency of Rossby wave breaking in this dynamically active region. Against this high background, the frequency of PV structure occurrence rises as genesis approaches, reaching 88% at lag 0. Following genesis, this association strengthens further, with PV occurrence increasing to over 94% by lag +2 for the surviving cloud bands. This suggests that while the presence of upstream PV structures is common, the sustained occurrence of PV structures is a characteristic feature of cloud band persistence.

This dependence on sustained forcing by PV structures is further clarified when stratifying by cloud band duration (Figure 6d). Long-lived (persistent) cloud band ($\geq$ 4 days) exhibit a consistently higher frequency of upstream PV structures throughout their lifetime, including the period before genesis, compared to short-lived events (1-2 days). From lag -7 to lag -1, the upstream environment of future persistent cloud bands is significantly more likely to contain a PV structure (frequency $\sim$0.88) than that of transient events ($\sim$0.84). The transitional (3-day) category consistently falls between these values, suggesting a coherent pattern where upstream PV frequency scales with cloud band duration. At genesis (lag 0), this distinction persists, with 90% of persistent events coinciding with a PV structure, compared to 88% for short-lived (transient) cloud bands. Post-genesis, the PV association for persistent cloud bands rises to and remains above 95% for several days, supporting the hypothesis that while the summer background state provides the necessary thermodynamic environment, sustained PV forcing is integral to maintaining cloud bands.

Spatial composites (Figure A2) visually and quantitatively confirm this persistence. For long-lived events, the composites reveal a coherent and intense upstream PV anomaly in PV structure occurrences that remains phase-locked with the cloud band centroid well into the mature and later stages of the lifecycle. This sustained upper-level support is accompanied by a distinct spatial pattern: persistent cloud bands maintain a significantly more zonal orientation (mean angle $\approx 57^\circ$ at lag +4) compared to the more meridionally orientated short-lived events ($\approx 51^\circ$ at genesis). This indicates that while short-lived cloud band events are associated with transient PV structures, long-lived cloud bands are associated with quasi-stationary PV structures that favour the zonally elongated shape of cloud bands

3.6.2 PV Depth and Latitudinal Position

Figure 6b displays the vertical depth of PV structures upstream of cloud bands. Following a period of nearly constant PV vertical depth, a deepening occurs coincident with cloud band genesis. The median depth increases at lag -1 (to 2.4 levels) and rises further to 2.55 levels at lag +1. Post-genesis, the median depth continues to increase for the surviving events, peaking at t+6 (2.63 levels). This trend suggests that while genesis is associated with a deepening PV structure, the subsequent deepening is a feature of the longest-lived events (yellow stars in Figure 6a). Stratifying by duration (Figure 6e) provides further context.

https://doi.org/10.5194/egusphere-2026-571
Preprint. Discussion started: 12 February 2026

While PV structures associated with long-lived cloud bands exhibit a higher median depth one week before genesis (2.41 levels at lag -7) compared to transient events (2.33 levels), the depths converge as genesis approaches, becoming nearly identical at onset (both ∼2.47 levels). The most notable difference is that PV structures in long-lived events maintain and increase their depth post-genesis. It is worth noting that transitional and long-lived (persistent) cloud bands dissipate after the peak in PV structure depth.

Regarding the meridional extent of these PV intrusions (Figure 6c), the median of the most equatorward latitude of the upstream PV structure remains stable at approximately 25.5°S from lag -7 to lag -2. An equatorward shift begins on the day before genesis (lag -1), reaching 23.5°S at genesis (lag 0). Crucially, while short-lived events exhibit a rapid, deep intrusion immediately following genesis (reaching 22.5°S at lag +1), this forcing is transient. In contrast, the equatorward intrusion for persistent cloud bands is sustained, progressively reaching 22.0°S by lag +5. The 90th percentile of the PV structures' most equatorward latitude ribbon further highlights the intensity of these intrusions; at genesis, 10% of events are associated with PV structures penetrating to 16.0°S, extending to 14.0°S by lag +5. This demonstrates that an important subset of cloud bands – likely clustered in the austral summer – is driven by deep intrusions of extratropical air into the tropics. Furthermore, long-lived cloud bands (Figure 6f) are distinguished by the latitudinal position of the PV structures. This configuration is established before genesis; at lag -2, PV structures for persistent cloud bands are already situated equatorward (24.5°S) of the peak latitude of transient events (26.0°S). This suggests that while short-lived events are driven by rapid, deep incursions of deep PV structures, long-lived cloud bands benefit from a favourable tropospheric environment where PV structures are already present at lower latitudes prior to genesis.

4 Conclusions

This study applies object-based algorithms for the identification of tropical–extratropical cloud bands and stratospheric potential vorticity (PV) structures to ERA5 reanalysis to clarify the influence of Rossby wave breaking on these cloud band characteristics over the South Pacific. We extend previous work by tracking cloud bands in time and by attributing these cloud bands to PV structures to elucidate the influence of extratropical forcing on the spatial distribution, seasonality, formation and maintenance of these cloud bands.

Our climatological analysis reveals that the spatial distribution of these features is not only aligned with the SPCZ, but also exhibits a statistically significant connection, confirming the critical role of these tropical–extratropical interactions in shaping regional cloudiness. Categorizing cloud band events by duration highlights distinct seasonal regimes: while short-lived cloud bands occur year-round, driven by transient, rapid PV intrusions, persistent cloud bands are strictly confined to the austral warm season. This seasonal confinement confirms that the maintenance of quasi-stationary tropical–extratropical cloud bands relies on the specific background state of the austral summer, characterized by the poleward excursion of the ITCZ and frequent intrusions of stratospheric PV into the tropical upper troposphere. The combination of this favourable thermodynamic environment with sustained upstream dynamic forcing allows for the maintenance of these systems over multiple days.

https://doi.org/10.5194/egusphere-2026-571
Preprint. Discussion started: 12 February 2026

Mechanistically, our composites corroborate the established framework whereby cyclonic PV anomalies steer moisture poleward and eastward, facilitating convection and shaping the characteristic diagonal orientation of cloud bands in the SPCZ.

A key novel finding of this study is that the lifetime of cloud bands depends on the sustained presence of dynamic forcing. While the South Pacific is a climatologically favourable region for Rossby wave breaking, we show that long-lived cloud bands are distinguished by a higher frequency of upstream PV structures persisting throughout the cloud band lifecycle. Furthermore, the initiation of these persistent cloud band events requires PV structures that penetrate deep into the tropical upper troposphere. The subsequent evolution reveals distinct dynamic regimes: short-lived events resemble rapid "bursts", characterized by deep but transient PV structures extending into low latitudes and a significantly more meridional cloud band orientation. These cloud band events are quickly terminated by downstream ridging. In contrast, persistent cloud bands are maintained by quasi-stationary circulation patterns, whereby the upstream midlatitude forcing sustains the tropical convection over multiple days. This sustained interaction favours the development of larger, significantly more zonally extended cloud systems. This demonstrates that while equatorward-extending Rossby wave breaking events facilitate the cloud band genesis, sustained midlatitude forcing is necessary for maintaining cloud band systems over multiple days.

Nevertheless, a limitation of our methodology is that while cloud bands are tracked, the associated PV structures are identified based on instantaneous spatial collocation. Explicitly tracking the PV structures would allow for a finer distinction between cloud bands sustained by a single, persistent Rossby wave breaking event versus those maintained by a succession of breaking Rossby waves. Furthermore, such an approach would allow for a quantitative analysis of the co-evolution of the PV and cloud band and their respective orientations, confirming the dynamic linkage suggested by our spatial composites.

Building on this object-orientated framework provides a pathway to further investigate the coupling between these extratropical and tropical forcings, such as equatorial Rossby or Kelvin waves. Finally, expanding this analysis to longer timescales and assessing how these life cycles are modulated by the Madden–Julian Oscillation or the Interdecadal Pacific Oscillation offers a promising avenue to improve the understanding and predictability of hydro-meteorological characteristics of extremes in the South Pacific region.

Code and data availability. The ERA5 reanalysis data are publicly available from the Copernicus Climate Data Store (Hersbach et al., 2018). The EM-DAT data are publicly available from the Emergency Events Database website https://www.emdat.be (last accessed: 11th February 2026). The cloud band detection algorithm is available under a BSD 3-Clause License at https://github.com/romainpilon/cloudbandPy (last accessed: 11th February 2026). The code used for the data analysis and the figures is available under an MIT license on Zenodo at https://doi.org/10.5281/zenodo.18429494 (last accessed: 11th February 2026).

https://doi.org/10.5194/egusphere-2026-571
Preprint. Discussion started: 12 February 2026

Appendix A

A1 Collocation Method between Deep Potential Vorticity Structures and Tropical-Extratropical Cloud Bands

The main manuscript introduces a collocation method between deep potential vorticity structures and tropical-extratropical cloud bands to find connections between the two features.

A connection between a tropical-extratropical cloud band and a PV structure is determined through the following steps. First, PV structures with bounding boxes overlapping the cloud band's bounding box are identified. Next, among these, PV structures whose centroid lies west of the cloud band's diagonal transect (see Figure A1, area with hatching) are flagged as connected to the cloud band. If multiple PV structures meet the criterion, only one connection is counted to avoid overestimating connections.

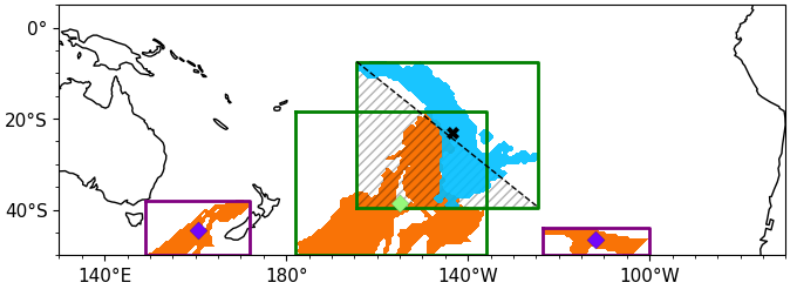

Figure A1. Daily snapshot of tropical-extratropical cloud bands (blue shading) and deep PV structures (orange shading) over the South Pacific on 21 January 2017. Green bounding boxes indicate overlapping cloud band and PV structure regions, while violet boxes show non-overlapping regions. The area with hatching represents the upstream sector for collocating PV structures. Diamond markers represent PV structure centroids, and crosses mark the cloud band centroid. Green centroids denote deep PV structures that satisfy both the overlap and 'west-to-cloud-band's-transect' criteria, i.e., within the cloud band upstream sector. Note that deep PV structures smaller than 10 pixels are omitted from this figure for visual clarity, though they are fully included in the collocation analysis.

A2 Spatial Composites Following the Tracked Cloud Bands

Figure A2 presents extended spatial composites of absolute PV depth anomalies and frequency of cloud band occurrence centred on the tracked cloud bands, spanning from genesis (lag 0) to 6 days after genesis (lag +6). These composites complement the statistical time series shown in Figure 6 by providing a horizontal map view of the evolving dynamic environment.

This figure confirms that the positive PV anomaly (red shading) in the upstream southwest sector is not a transient feature limited to genesis but remains a coherent, phase-locked structure that co-evolves with long-lived cloud bands well into their decay phase. Furthermore, cloud band orientation (α) is found to be significantly more zonal for persistent events (mean angle $\sim$56–58°) than for the more meridionally tilted short-lived events ($\sim$51–53°).

https://doi.org/10.5194/egusphere-2026-571
Preprint. Discussion started: 12 February 2026

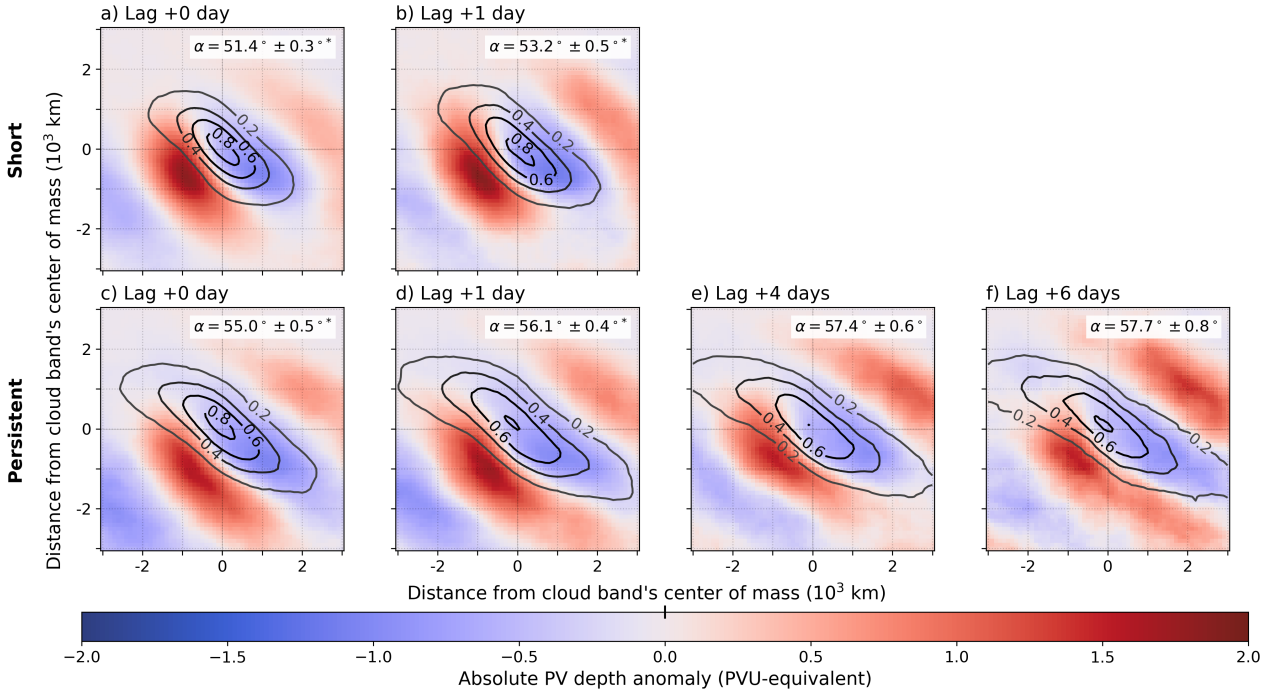

Figure A2. Time-lagged horizontal composites of absolute PV depth anomalies (shading) and relative frequency of cloud band occurrence (contours) centred on the tracked cloud band centroid for positive lags and the genesis position for negative lags. The composites are stratified by cloud band duration: (a-b) short-lived cloud bands (duration 1–2 days) and (c-f) persistent cloud bands (duration $\geq$ 4 days). The PV anomalies are calculated as the daily PV depth minus the long-term climatological mean (1959–2021) based on a 21-day running mean of daily average. Cloud band frequency contours are shown at intervals of 0.2, starting at 0.2. The reference frame moves with the cloud band centroid at each lag. The mean cloud band orientation angle (α) is annotated in each panel with its standard error. The angle is measured such that 90° represents a purely zonal/East-West orientation and 0° represents North-South. Asterisks (*) indicate a statistically significant difference in orientation between short and persistent events at the 99% confidence level ($p < 0.01$) using a Welch's t-test.

Author contributions. RP designed the study. RP, AJDV and DD contributed to the interpretation of the results. RP performed all analyses and wrote the paper, based on discussions with and input from all co-authors; AJDV and DD provided critical feedback, reviewed and edited the manuscript until its final version. DD secured the funding.

Competing interests. At least one of the (co-)authors is a member of the editorial board of Weather and Climate Dynamics.

Acknowledgements. Support from the Swiss National Science Foundation through project PP00P2_198896 to Daniela I. V. Domeisen is gratefully acknowledged. A large language model was used for linguistic refinement and to speed up coding for plotting.

https://doi.org/10.5194/egusphere-2026-571
Preprint. Discussion started: 12 February 2026

References

Allen, G., Vaughan, G., Brunner, D., T. May, P., Heyes, W., Minnis, P., and K. Ayers, J.: Modulation of tropical convection by breaking Rossby waves, Quarterly Journal of the Royal Meteorological Society, 135, 125–137, https://doi.org/https://doi.org/10.1002/qj.349, 2009.

Appenzeller, C. and Davies, H. C.: Structure of stratospheric intrusions into the troposphere, Nature, 358, 570–572, https://doi.org/10.1038/358570a0, 1992.

Black, A. S., Risbey, J. S., Chapman, C. C., Monselesan, D. P., II, T. S. M., Pook, M. J., Richardson, D., Sloyan, B. M., Squire, D. T., and Tozer, C. R.: Australian Northwest Cloudbands and Their Relationship to Atmospheric Rivers and Precipitation, Monthly Weather Review, 149, 1125 – 1139, https://doi.org/10.1175/MWR-D-20-0308.1, 2021.

Brown, J. R., Lengaigne, M., Lintner, B. R., Widlansky, M. J., van der Wiel, K., Dutheil, C., Linsley, B. K., Matthews, A. J., and Renwick, J.: South Pacific Convergence Zone dynamics, variability and impacts in a changing climate, Nature Reviews Earth and Environment, 1, 530–543, https://doi.org/10.1038/s43017-020-0078-2, 2020.

de Vries, A. J., Feldstein, S. B., Riemer, M., Tyrlis, E., Sprenger, M., Baumgart, M., Fnais, M., and Lelieveld, J.: Dynamics of tropical–extratropical interactions and extreme precipitation events in Saudi Arabia in autumn, winter and spring, Quarterly Journal of the Royal Meteorological Society, 142, 1862–1880, https://doi.org/https://doi.org/10.1002/qj.2781, 2016.

de Vries, A. J., Ouwersloot, H. G., Feldstein, S. B., Riemer, M., El Kenawy, A. M., McCabe, M. F., and Lelieveld, J.: Identification of Tropical-Extratropical Interactions and Extreme Precipitation Events in the Middle East Based On Potential Vorticity and Moisture Transport, Journal of Geophysical Research: Atmospheres, 123, 861–881, https://doi.org/https://doi.org/10.1002/2017JD027587, 2018.

de Vries, A. J., Armon, M., Klingmüller, K., Portmann, R., Röthlisberger, M., and Domeisen, D. I. V.: Breaking Rossby waves drive extreme precipitation in the world's arid regions, Communications Earth & Environment, 5, 493, https://doi.org/10.1038/s43247-024-01633-y, 2024.

Delforge, D., Wathelet, V., Below, R., Lanfredi Sofia, C., Tonnelier, M., van Loenhout, J. A. F., and Speybroeck, N.: The EM-DAT Emergency Events Database Archive [Dataset], https://doi.org/https://doi.org/10.14428/DVN/I0LTPH, 2024.

Fröhlich, L. and Knippertz, P.: Identification and global climatology of upper-level troughs at low latitudes, Meteorologische Zeitschrift, 17, 565–573, https://doi.org/10.1127/0941-2948/2008/0320, 2008.

Fröhlich, L., Knippertz, P., Fink, A. H., and Hohberger, E.: An Objective Climatology of Tropical Plumes, Journal of Climate, 26, 5044 – 5060, https://doi.org/10.1175/JCLI-D-12-00351.1, 2013.

Funatsu, B. M. and Waugh, D. W.: Connections between Potential Vorticity Intrusions and Convection in the Eastern Tropical Pacific, Journal of the Atmospheric Sciences, 65, 987 – 1002, https://doi.org/10.1175/2007JAS2248.1, 2008.

Griffiths, G. M., Salinger, M. J., and Leleu, I.: Trends in extreme daily rainfall across the South Pacific and relationship to the South Pacific Convergence Zone, International Journal of Climatology, 23, 847–869, https://doi.org/https://doi.org/10.1002/joc.923, 2003.

Hart, N. C. G., Reason, C. J. C., and Fauchereau, N.: Cloud bands over southern Africa: seasonality, contribution to rainfall variability and modulation by the MJO, Climate Dynamics, 41, 1199–1212, https://doi.org/10.1007/s00382-012-1589-4, 2013.

Hart, R. E. and Grumm, R. H.: Using Normalized Climatological Anomalies to Rank Synoptic-Scale Events Objectively, Monthly Weather Review, 129, 2426 – 2442, https://doi.org/10.1175/1520-0493(2001)129<2426:UNCATR>2.0.CO;2, 2001.

Hersbach, H., Bell, B., Berrisford, P., Biavati, G., Horányi, A., Muñoz Sabater, J., Nicolas, J., Peubey, C., Radu, R., Rozum, I., Schepers, D., Simmons, A., Soci, C., Dee, D., and Thépaut, J.-N.: ERA5 hourly data on single levels from 1940 to present. Copernicus Climate Change Service (C3S) Climate Data Store (CDS), https://doi.org/10.24381/cds.adbb2d47, 2018.

https://doi.org/10.5194/egusphere-2026-571
Preprint. Discussion started: 12 February 2026

Hersbach, H., Bell, B., Berrisford, P., Hirahara, S., Horányi, A., Muñoz-Sabater, J., Nicolas, J., Peubey, C., Radu, R., Schepers, D., Simmons, A., Soci, C., Abdalla, S., Abellan, X., Balsamo, G., Bechtold, P., Biavati, G., Bidlot, J., Bonavita, M., De Chiara, G., Dahlgren, P., Dee, D., Diamantakis, M., Dragani, R., Flemming, J., Forbes, R., Fuentes, M., Geer, A., Haimberger, L., Healy, S., Hogan, R. J., Hólm, E., Janisková, M., Keeley, S., Laloyaux, P., Lopez, P., Lupu, C., Radnoti, G., de Rosnay, P., Rozum, I., Vamborg, F., Villaume, S., and Thépaut, J.-N.: The ERA5 global reanalysis, Quarterly Journal of the Royal Meteorological Society, 146, 1999–2049, https://doi.org/10.1002/qj.3803, 2020.

Kiladis, G. N.: Observations of Rossby Waves Linked to Convection over the Eastern Tropical Pacific, Journal of the Atmospheric Sciences, 55, 321–339, https://doi.org/https://doi.org/10.1175/1520-0469(1998)055<0321:OORWLT>2.0.CO;2, 1998.

Kiladis, G. N. and Weickmann, K. M.: Extratropical Forcing of Tropical Pacific Convection during Northern Winter, Monthly Weather Review, 120, 1924–1939, https://doi.org/https://doi.org/10.1175/1520-0493(1992)120<1924:EFOTPC>2.0.CO;2, 1992.

Knippertz, P.: Tropical–extratropical interactions related to upper-level troughs at low latitudes, Dynamics of Atmospheres and Oceans, 43, 36–62, https://doi.org/https://doi.org/10.1016/j.dynatmoce.2006.06.003, current Contributions to Understanding the General Circulation of the Atmosphere, 2007.

Knippertz, P. and Martin, J. E.: Tropical plumes and extreme precipitation in subtropical and tropical West Africa, Quarterly Journal of the Royal Meteorological Society, 131, 2337–2365, https://doi.org/https://doi.org/10.1256/qj.04.148, 2005.

Kodama, Y.: Large-Scale Common Features of Subtropical Precipitation Zones (the Baiu Frontal Zone, the SPCZ, and the SACZ) Part I: Characteristics of Subtropical Frontal Zones, Journal of the Meteorological Society of Japan. Ser. II, 70, 813–836, https://doi.org/10.2151/jmsj1965.70.4_813, 1992.

Kumar, V. V., Deo, R. C., and Ramachandran, V.: Total rain accumulation and rain-rate analysis for small tropical Pacific islands: a case study of Suva, Fiji, Atmospheric Science Letters, 7, 53–58, https://doi.org/https://doi.org/10.1002/asl.131, 2006.

Lorrey, A., Dalu, G., Renwick, J., Diamond, H., and Gaetani, M.: Reconstructing the South Pacific Convergence Zone Position during the Presatellite Era: A La Niña Case Study, Monthly Weather Review, 140, 3653 – 3668, https://doi.org/10.1175/MWR-D-11-00228.1, 2012.

Matthews, A. J.: A multiscale framework for the origin and variability of the South Pacific Convergence Zone, Quarterly Journal of the Royal Meteorological Society, 138, 1165–1178, https://doi.org/https://doi.org/10.1002/qj.1870, 2012.

Matthews, A. J., Hoskins, B. J., Slingo, J. M., and Blackburn, M.: Development of convection along the SPCZ within a Madden-Julian oscillation, Quarterly Journal of the Royal Meteorological Society, 122, 669–688, https://doi.org/https://doi.org/10.1002/qj.49712253106, 1996.

McIntyre, M. E. and Palmer, T. N.: Breaking planetary waves in the stratosphere, Nature, 305, 593–600, https://doi.org/10.1038/305593a0, 1983.

Murthy, V. S. and Boos, W. R.: Understanding the vertical structure of potential vorticity in tropical depressions, Quarterly Journal of the Royal Meteorological Society, 145, 1968–1991, https://doi.org/https://doi.org/10.1002/qj.3539, 2019.

Niznik, M., Lintner, B. R., Matthews, A. J., and Widlansky, M. J.: The Role of Tropical–Extratropical Interaction and Synoptic Variability in Maintaining the South Pacific Convergence Zone in CMIP5 Models, Journal of Climate, 28, 3353 – 3374, https://doi.org/10.1175/JCLI-D-14-00527.1, 2015.

Oertel, A., Boettcher, M., Joos, H., Sprenger, M., and Wernli, H.: Potential vorticity structure of embedded convection in a warm conveyor belt and its relevance for large-scale dynamics, Weather and Climate Dynamics, 1, 127–153, https://doi.org/10.5194/wcd-1-127-2020, 2020.

https://doi.org/10.5194/egusphere-2026-571
Preprint. Discussion started: 12 February 2026

Pilon, R. and Domeisen, D. I. V.: cloudbandPy 1.0: an automated algorithm for the detection of tropical–extratropical cloud bands, Geoscientific Model Development, 17, 2247–2264, https://doi.org/10.5194/gmd-17-2247-2024, 2024.

Portmann, R., Sprenger, M., and Wernli, H.: The three-dimensional life cycles of potential vorticity cutoffs: a global and selected regional climatologies in ERA-Interim (1979–2018), Weather and Climate Dynamics, 2, 507–534, https://doi.org/10.5194/wcd-2-507-2021, 2021.

Rosa, E. B., Pezzi, L. P., Quadro, M. F. L. d., and Brunsell, N.: Automated Detection Algorithm for SACZ, Oceanic SACZ, and Their Climatological Features, Frontiers in Environmental Science, 8, https://doi.org/10.3389/fenvs.2020.00018, original Research, 2020.

Sagero, P. O., Pratap, A., Magiri, R., Ongoma, V., and Okello, P.: Validation of ERA5 rainfall data over the South Pacific Region: case study of Fiji Islands, Meteorology and Atmospheric Physics, 136, 28, https://doi.org/10.1007/s00703-024-01025-z, 2024.

Stan, C., Straus, D. M., Frederiksen, J. S., Lin, H., Maloney, E. D., and Schumacher, C.: Review of Tropical-Extratropical Teleconnections on Intraseasonal Time Scales, Reviews of Geophysics, 55, 902–937, https://doi.org/https://doi.org/10.1002/2016RG000538, 2017.

Takahashi, K. and Battisti, D. S.: Processes Controlling the Mean Tropical Pacific Precipitation Pattern. Part II: The SPCZ and the Southeast Pacific Dry Zone, Journal of Climate, 20, 5696 – 5706, https://doi.org/10.1175/2007JCLI1656.1, 2007.

Telcik, N. and Pattiaratchi, C.: Influence of Northwest Cloudbands on Southwest Australian Rainfall, Journal of Climatology (Cairo), 2014, 671 394, https://doi.org/https://doi.org/10.1155/2014/671394, 2014.

Thorncroft, C. D., Hoskins, B. J., and McIntyre, M. E.: Two paradigms of baroclinic-wave life-cycle behaviour, Quarterly Journal of the Royal Meteorological Society, 119, 17–55, https://doi.org/https://doi.org/10.1002/qj.49711950903, 1993.

Tubi, A. and Dayan, U.: Tropical Plumes over the Middle East: Climatology and synoptic conditions, Atmospheric Research, 145-146, 168–181, https://doi.org/https://doi.org/10.1016/j.atmosres.2014.03.028, 2014.

van der Wiel, K., Matthews, A. J., Stevens, D. P., and Joshi, M. M.: A dynamical framework for the origin of the diagonal South Pacific and South Atlantic Convergence Zones, Quarterly Journal of the Royal Meteorological Society, 141, 1997–2010, https://doi.org/https://doi.org/10.1002/qj.2508, 2015.

van der Wiel, K., Matthews, A. J., Joshi, M. M., and Stevens, D. P.: Why the South Pacific Convergence Zone is diagonal, Climate Dynamics, 46, 1683–1698, https://doi.org/10.1007/s00382-015-2668-0, 2016.

Vincent, D. G.: The South Pacific Convergence Zone (SPCZ): A Review, Monthly Weather Review, 122, 1949 – 1970, https://doi.org/10.1175/1520-0493(1994)122<1949:TSPCZA>2.0.CO;2, 1994.

Waugh, D. W. and Funatsu, B. M.: Intrusions into the Tropical Upper Troposphere: Three-Dimensional Structure and Accompanying Ozone and OLR Distributions, Journal of the Atmospheric Sciences, 60, 637 – 653, https://doi.org/10.1175/1520-0469(2003)060<0637:IITTUT>2.0.CO;2, 2003.

Waugh, D. W. and Polvani, L. M.: Climatology of intrusions into the tropical upper troposphere, Geophysical Research Letters, 27, 3857–3860, https://doi.org/https://doi.org/10.1029/2000GL012250, 2000.

Webster, P. J. and Holton, J. R.: Cross-Equatorial Response to Middle-Latitude Forcing in a Zonally Varying Basic State, Journal of Atmospheric Sciences, 39, 722 – 733, https://doi.org/10.1175/1520-0469(1982)039<0722:CERTML>2.0.CO;2, 1982.

Wernli, H. and Sprenger, M.: Identification and ERA-15 Climatology of Potential Vorticity Streamers and Cutoffs near the Extratropical Tropopause, Journal of the Atmospheric Sciences, 64, 1569 – 1586, https://doi.org/10.1175/JAS3912.1, 2007.

Widlansky, M. J., Webster, P. J., and Hoyos, C. D.: On the location and orientation of the South Pacific Convergence Zone, Climate Dynamics, 36, 561–578, https://doi.org/10.1007/s00382-010-0871-6, 2011.

Zilli, M. T. and Hart, N. C. G.: Rossby Wave Dynamics over South America Explored with Automatic Tropical–Extratropical Cloud Band Identification Framework, Journal of Climate, 34, 8125 – 8144, https://doi.org/10.1175/JCLI-D-21-0020.1, 2021.

https://doi.org/10.5194/egusphere-2026-571
Preprint. Discussion started: 12 February 2026

Zilli, M. T., Hart, N. C. G., Coelho, C. A. S., Chadwick, R., de Souza, D. C., Kubota, P. Y., Figueroa, S. N., and Cavalcanti, I. F. A.: Characteristics of tropical–extratropical cloud bands over tropical and subtropical South America simulated by BAM-1.2 and HadGEM3-GC3.1, Quarterly Journal of the Royal Meteorological Society, 149, 1498–1519, https://doi.org/https://doi.org/10.1002/qj.4470, 2023.